JMEPEG (2010) 19:1311–1317
DOI: 10.1007/s11665-010-9631-3

1059-9495/$19.00

Passivity and Pitting Corrosion of X80 Pipeline Steel in Carbonate/Bicarbonate Solution Studied by Electrochemical Measurements

H.B. Xue and Y.F. Cheng

(Submitted September 23, 2009; in revised form February 17, 2010)

This work investigated the effects of chloride ions and hydrogen-charging on the passivity and pitting corrosion behavior of X80 pipeline steel in a bicarbonate-carbonate solution by electrochemical and photo-electrochemical techniques. It was found that a stable passivity can be established on the steel in the absence and presence of chloride ions. The hydrogen-charging does not alter the transpassive potential, but increases the passive current density. When chloride ions are contained in the solution, pitting corrosion will be initiated. The pitting potential is independent of the hydrogen-charging. Hydrogen-charging would enhance the anodic dissolution and electrochemical activity of the steel, but does not affect the pitting potential, which indicates that the charged hydrogen is not involved in the pitting initiation. However, hydrogen may accelerate the pit growth. Photo illumination could enhance the activity of the steel electrode, resulting in an increase of photo-induced anodic current density.

Keywords bicarbonate-carbonate solution, passivity, pitting corrosion, X80 steel

1. Introduction

It has been acknowledged (Ref 1-16) that a majority of pipeline stress corrosion cracking (SCC) occurs under a high pH condition, which is associated with a concentrated carbonate/bicarbonate solution with a pH of about 9.5. The high pH SCC of pipelines is believed to be due to the selective dissolution and repeated rupture of passive film along grain boundaries (Ref 3, 7-9). Generally, pipeline steel can be passivated in the concentrated carbonate/bicarbonate solution (Ref 17-19). In the presence of aggressive species, i.e., Cl^- ions, the passive film may be broken to initiate pitting corrosion. It has been reported (Ref 20, 21) that corrosion pits are usually the incubators of stress corrosion cracks in pipeline steel.

It has been demonstrated (Ref 22-26) that the passive film formed on pipeline steel in concentrated bicarbonate/carbonate solution behave like a semiconductor, and the semiconducting properties of the film play an essential role in corrosion and SCC processes of the steel (Ref 27, 28). Furthermore, the presence of hydrogen in pipeline steel influences strongly its chemical and mechanical properties (Ref 29-32). Also, the transport of hydrogen through passive film affects many corrosion processes, such as pitting corrosion and SCC (Ref 29, 32). Recent investigations (Ref 33, 34) showed that hydrogen, as a product of corrosion reaction, has significant influence on the composition and structure of passive film, and results in an increased pitting susceptibility and a decreased corrosion resistance of the film.

Photo-electrochemical technique provides a promising alternative to study the semiconducting properties of passive film, and simultaneously, to characterize in situ the effect of hydrogen in steel on its corrosion and cracking behavior (Ref 35-38). For example, Razzini et al. (Ref 35) used a photo-electrochemical microscopy (PEM) to image the distribution of hydrogen at the crack tip in a loaded X60 pipe steel specimen after hydrogen-charging. It demonstrated that a large amount of hydrogen segregates at high stress regions. Zeng et al. (Ref 39, 40) used photo-electrochemical measurements to investigate the effects of hydrogen and chloride ions on the electronic properties of passive film on X70 steel in 0.5 M $NaHCO_3$ solution. It found that hydrogen could promote localized corrosion.

The X80 steel is a high-strength steel and is being used in pipeline operations in Arctic and sub-Arctic areas (Ref 41). Development of an advanced understanding of the corrosion and SCC behavior of X80 steel is critical to the safe operation of pipelines. In this work, the passivity and pitting corrosion behavior of X80 steel were investigated in a carbonate/bicarbonate solution by electrochemical and photo-electrochemical measurements. The effects of chloride ions and hydrogen on the properties of passive film and pitting corrosion were determined.

2. Experimental

2.1 Electrodes and Solutions

The specimens used for this work were a X80 steel, with the chemical composition (wt.%): C 0.026, Mn 1.6, Si 0.22,

H.B. Xue and **Y.F. Cheng**, Department of Mechanical and Manufacturing Engineering, University of Calgary, Calgary, AB T2N 1N4, Canada. Contact e-mail: fcheng@ucalgary.ca.

S 0.001, P 0.003, Ni 0.15, Cr 0.27, Cu 0.27, Nb 0.097, Ti 0.014, and Fe balance. The specimens were ground to 1200 grit SiC paper, degreased in acetone, cleaned with distilled water, and then dried in cold air.

The test solutions contained 1 M $NaHCO_3$ + 0.5 M Na_2CO_3 solution without and with the addition of 0.01 M NaCl, with pH values of 9.53 and 9.48, respectively. For hydrogen-charging, a diluted bicarbonate solution, with the chemical composition of 0.483 g/L $NaHCO_3$, 0.122 g/L KCl, 0.181 g/L $CaCl_2 \cdot 2H_2O$, and 0.131 g/L $MgSO_4 \cdot 7H_2O$, was used. Prior to charging, the solution was purged with 5% CO_2/N_2 for 1 h to remove oxygen, and the gas flow was maintained through the charging process. All solutions were made from analytic grade reagents (Fisher Scientific) and ultra-pure water (18 MΩ cm in resistivity). All tests were carried out at room temperature (~22 °C).

2.2 Design of PEC System and Photo-Current Measurements

The hydrogen-charging was carried out through a Devanathan-Stachurski cell, which was comprised of two compartments separated by the X80 steel specimen, with an exposed working area of 1 cm^2 and a thickness of 0.1 cm. The hydrogen-charging side was polarized galvanostatically with a cathodic current density of 10 mA/cm^2 for 2 h. After charging, the steel specimen at the test cell was polarized potentiostatically at 0.15 V (saturated calomel electrode, SCE) for 3600 s. A laser illumination was then conducted on the specimen surface to measure the photo-current through a home-developed PEC system, which was composed of a 500 mW Argon ion laser source (Model 5490A ILT 6000 series, Ion Laser Technology Inc., USA) with a wavelength range of 457 to 514 nm. The generated photo-current was recorded by a PARSTAT 263A potentiostat.

2.3 Electrochemical Measurements

Prior to electrochemical measurement, corrosion potential of the steel electrode was monitored through a Solartron 1280C electrochemical system in the test solution until a steady-state value was reached. The electrochemical impedance spectroscopy (EIS) measurement was then conducted through a Solartron 1280C electrochemical system, using a typical three-electrode system, with the steel specimen as working electrode (WE), a SCE as reference electrode and a platinum sheet as counter electrode. The measurement frequency ranged from 0.01 to 20,000 Hz with an applied AC amplitude of 5 mV.

Potentiodynamic polarization curve was measured through the Solartron 1280C electrochemical system with a potential scanning rate of 20 mV/min.

Cyclic polarization test was started at 20 mV below corrosion potential (E_{corr}) and scanned at a rate of 1 mV/s in the positive direction until an anodic threshold current density of 0.2 mA/cm^2 was reached. The scan then was reversed to E_{corr}. The cyclic polarization measurements were performed through a Reference 600 Gamry electrochemical measurement system.

2.4 Pit Propagation Rate Test

The pit propagation rate (PPR) test was a method in which the specimen was subjected to a potential cycle, and was performed by the Potential Scan/Hold module of the Solartron 1280C electrochemical system. The potential was first potentiodynamically scanned at a rate of 10 mV/s from E_{corr} to a passive potential of 0.2 V (SCE), which was between the protection potential, E_p, and the pitting potential, E_{pit}, as determined in the measured cyclic polarization curves, where E_{pit} refers to the potential below which no new pit initiates and only the existing pits grow, and E_p refers to the potential below which the existing pits will be repassivated. After holding at this potential for 10 min to obtain a steady-state current density, the potential scan was continued to a potential more noble than E_{pit}, where the current density reached a value of 1 mA/cm^2, corresponding to the stable growth of corrosion pits. The potential was then back in a single step to 0.2 V (SCE) and held for 10 min. Since there was no new stable pit generating at potential below E_{pit}, the recorded current density was a summation of the current density of existing pit growth and dissolution current density of the steel at the passive potential. The potential was then shifted negatively to a value of −0.1 V (SCE), and held for 10 min in order to repassivate the existing pits. The potential was scanned to 0.2 V (SCE) again to check the repassivation of pits.

The measurements were conducted on X80 steel electrodes without and with hydrogen pre-charging, and the results were determined by graphic integration of the measured current density versus time data.

2.5 Mott-Schottky Analysis

In order to obtain Mott-Schottky plots for X80 steel in the test solution, the electrode was pre-polarized at a film-formation potential of 0.15 V (SCE) for 3600 s, and the capacitance measurement was then conducted at a potential scanning speed of 40 mV/s from −0.4 to 0.6 V (SCE) in the anodic direction through the Solartron 1280C electrochemical system. An AC signal with amplitude of 5 mV was applied, and the measuring frequency was 1000 Hz.

3. Results

3.1 Corrosion Potential Measurements

Figure 1 shows the time dependences of corrosion potentials measured on the uncharged and charged X80 steel electrode in the solution without and with 0.01 M NaCl. It is seen that hydrogen-charging would shift the steady-state corrosion potential of the steel negatively. Moreover, an addition of chloride ions shifted the corrosion potential to the negative direction. Therefore, both the Cl^- ion addition and hydrogen-charging would enhance the electrochemical activity of the steel.

3.2 EIS Measurements

Figure 2 shows the EIS plots (a—Nyquist diagram, b—Bode diagram) measured on the uncharged and charged X80 steel electrodes in the solution without and with Cl^- ions. It is seen that all EIS plots were featured with a depressed semicircle loop over the whole frequency range. Moreover, hydrogen-charging and chloride ion addition would decrease the size of the semicircle. Correspondingly, the low-frequency impedances measured in Bode diagram decreased obviously with the presence of Cl^- ions and the hydrogen-charging.

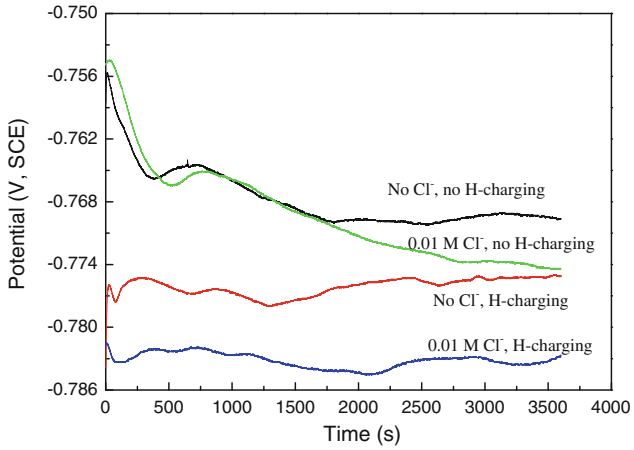

Fig. 1 Time dependence of corrosion potentials measured on the uncharged and pre-charged steel electrodes in the solutions without and with 0.01 M NaCl

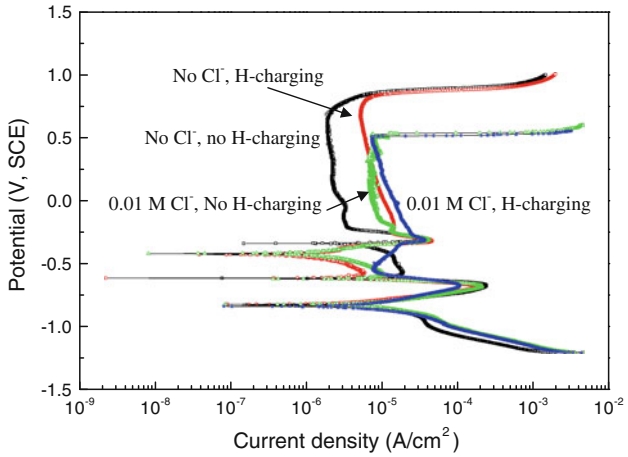

Fig. 3 Polarization curves measured on the uncharged and pre-charged steel electrodes in the solutions without and with 0.01 M NaCl

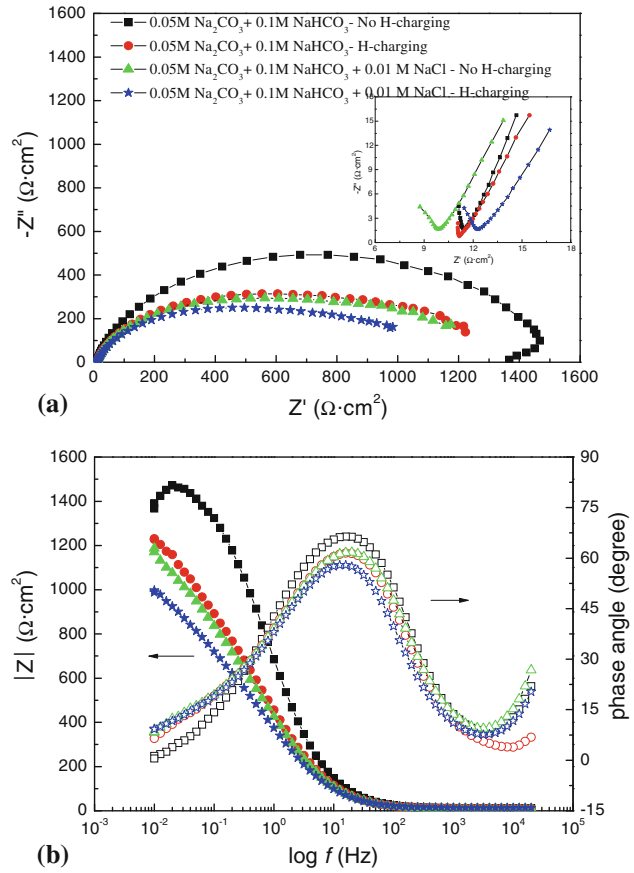

Fig. 2 EIS plots measured on the uncharged and pre-charged steel electrodes in the solutions without and with 0.01 M NaCl (a) Nyquist diagram; (b) Bode diagram (Inset figure is the enlarged EIS plots in the high frequency range)

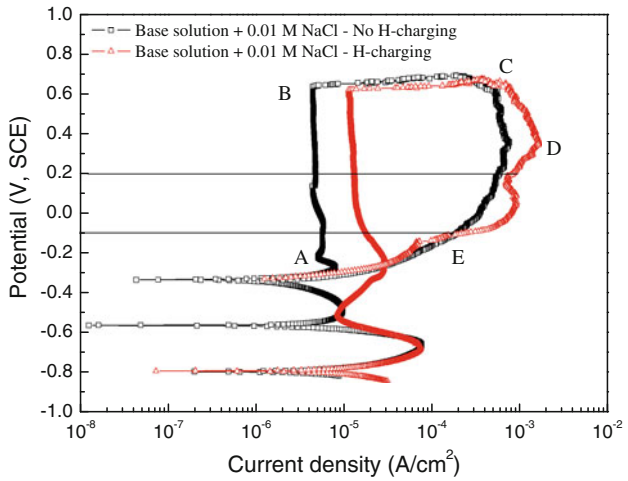

Fig. 4 Cyclic polarization curves measured on the uncharged and pre-charged electrodes in the base solution containing 0.01 M NaCl

3.3 Potentiodynamic Polarization and Cyclic Polarization Measurements

Figure 3 shows the potentiodynamic polarization curves of the uncharged and charged X80 steel in the test solution without and with addition of chloride ions. It is seen that a stable passivity could be developed on the steel in all solutions. Upon hydrogen-charging, there was an apparent increase of the passive current density. However, the E_{pit} kept unchanged. With the addition of chloride ions, the passive current density increased, and simultaneously, the E_{pit} was shifted negatively and the passive range decreased.

Figure 4 shows the cyclic polarization curves of the uncharged and charged X80 steel electrodes in the test solution containing 0.01 M NaCl. It is seen that both curves exhibited a big hysteresis loop. Electrochemical cyclic polarization measurement is capable of predicting the susceptibility of a passivated metal to pitting corrosion. Generally, if the reverse anodic curve is shifted to higher currents than the forward curve, i.e., positive hysteresis, pitting corrosion will occur. It is apparent from Fig. 4 that positive hysteresis loops are measured under both conditions, suggesting that pitting of X80 steel is inevitable in the test systems. The steel was in a stable passivity in the potential region AB. When the applied potential exceeded the point B, i.e., E_{pit}, pitting was initiated, followed by a rapid current increase in the region BC. The current was

reversely scanned at a current density of 0.2 mA/cm^2 at point C. In region CD, the generated pits continued to grow, resulting in the increase of current density. The current density decreased in the region DE, indicating that corrosion pits were partially repassivated. Furthermore, upon hydrogen-charging, the passive current density increased. However, there was little change of the E_{pit}.

3.4 Pit Propagation Rate Tests

Figure 5 shows the current density profiles of the charged and uncharged X80 steels in a potential step cycle in the chloride-containing solution. When the potential was scanned from E_{corr} to 0.2 V (SCE), which was in the passive region as seen in Fig. 3, the current density increased initially, and then dropped gradually to a steady value, which is indicated clearly in Fig. 5(b). The steel electrode was in passivity at 0.2 V (SCE) and the anodic current density was kept at a low, steady-state value. When the potential was shifted from 0.2 V (SCE) to 0.8 V (SCE), a potential more positive than E_{pit} that was about 0.6 V (SCE), the current density increased rapidly. When potential was back in a single step to 0.2 V (SCE) and held for 10 min, the current density continued to increase and fluctuated around a relatively stable value. After the potential was shifted negatively to −0.1 V (SCE), and held for 10 min, the current density decreased and maintained at a low value. When potential was increased to 0.2 V (SCE) again, the current density increased rapidly to a higher value than that recorded previously at the same potential.

Moreover, compared to the current density measured on the uncharged electrode, there was a high current density obtained on the charged electrode.

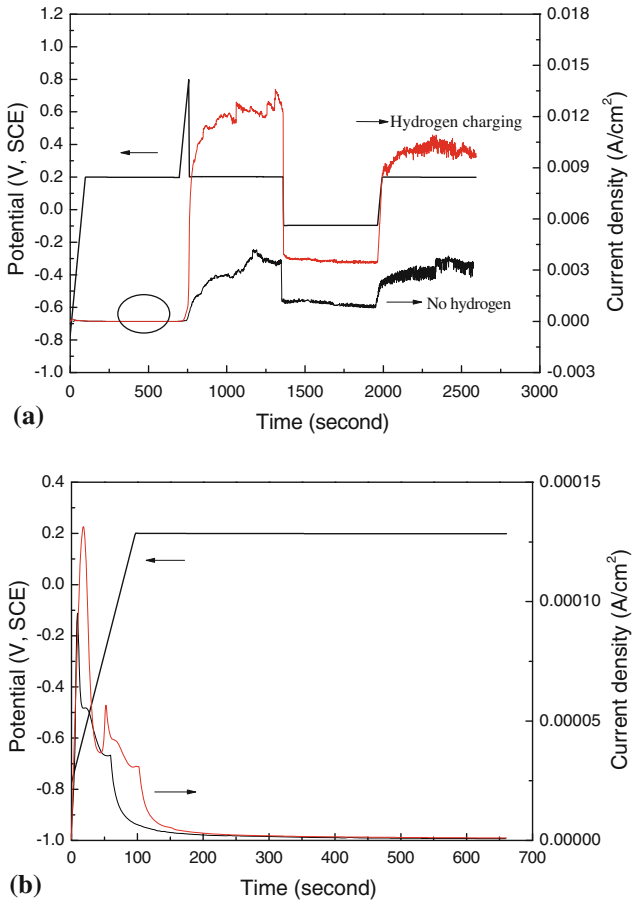

Fig. 5 Potential-time and current density-time curves in PPR tests, where (b) is the enlarged plots of the passive current densities in (a)

3.5 Capacitance Measurement and Mott-Schottky Analysis

Figure 6 shows the Mott-Schottky plots measured on the uncharged and pre-charged electrodes in the solutions without and with 0.01 M NaCl. It is seen that the slopes of all plots were positive, indicating an n-type semiconductor of the passive films formed on the steel. Moreover, a non-linear behavior was observed in the Mott-Schottky plots. Furthermore, the measured space-charge layer capacitance increased upon hydrogen-charging and the chloride addition. The slope of the Mott-Schottky plot decreased with the addition of Cl^- and hydrogen-charging.

3.6 Photo-Current Measurements

Figure 7 shows the effect of photo illumination on anodic current densities of the uncharged and charged electrodes

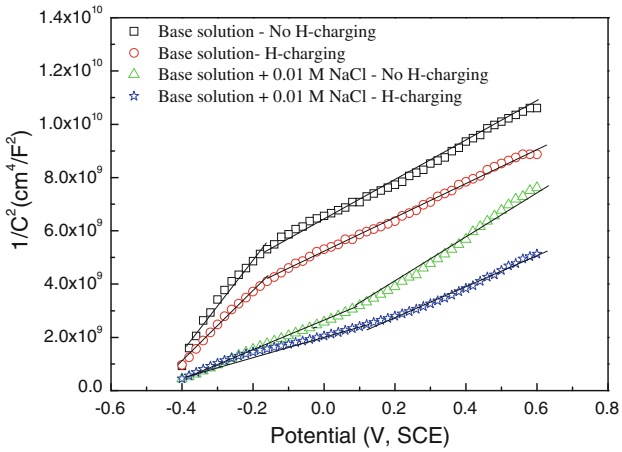

Fig. 6 Mott-Schottky plots measured on the uncharged and pre-charged electrodes in the solutions without and with 0.01 M NaCl

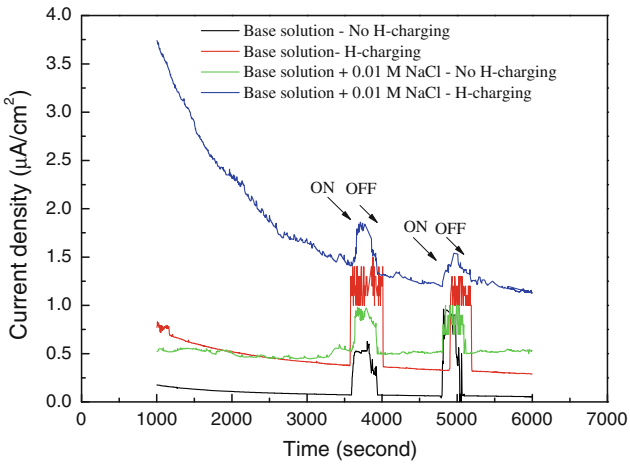

Fig. 7 Current densities of the uncharged and pre-charged electrodes in the solutions without and with 0.01 M NaCl under photo illumination

potentiostatically polarized at a film-formation potential of 0.15 V (SCE) in the solution without and with Cl^-. It is seen that the anodic current densities for both the uncharged and pre-charged electrodes increased upon photo illumination. When the laser source was turned off, the current density recovered to the original value. Moreover, the background anodic current density increased with pre-charging or the addition of chloride ions in the solution.

4. Discussion

4.1 Passivity and Pitting Corrosion of X80 Steel in Chloride-Containing Bicarbonate-Carbonate Solution

Author' previous study (Ref 42) has demonstrated that the pipeline steels, such as X70 steel, can be passivated in carbonate-bicarbonate solution. The present work shows that a stable passivity can be established on X80 steel in the solution. Upon immersion of the steel in solution and the positive shift of applied potential, the active dissolution of the steel results in the increase of current density, where the steel is in an activation state. With the increase of potential, a dissolvable $FeCO_3$ deposit layer is formed on the steel surface, resulting in the generation of a current peak at about −0.75 V (SCE) in Fig. 3 (Ref 19, 43):

$$Fe + HCO_3^- \rightarrow FeCO_3 + H^+ + 2e \quad \text{(Eq 1)}$$

With the further increase of anodic potential, the second current peak is observed at about −0.3 V (SCE). It is due to the oxidation of ferrous species, $FeCO_3$, to Fe_2O_3 and Fe_3O_4 (Ref 44-47):

$$4FeCO_3 + O_2 + 4H_2O \rightarrow 2Fe_2O_3 + 4HCO_3^- + 4H^+ \quad \text{(Eq 2)}$$

$$6FeCO_3 + O_2 + 6H_2O \rightarrow 2Fe_3O_4 + 6HCO_3^- + 6H^+ \quad \text{(Eq 3)}$$

In the absence of chloride ions, the rapid increase of current density above 0.8 V (SCE) is due to the transpassive dissolution of Fe into Fe^{3+} and, simultaneously, the evolution of oxygen by the water oxidation. The hydrogen-charging will not alter the transpassive potential, but increase the anodic current density, as seen in Fig. 3. When chloride ions are contained in the solution, pitting corrosion will be initiated when the anodic potential exceeds the E_{pit}, which is approximately 0.5-0.6 V (SCE). Similarly, a hydrogen-charging does not change the pitting potential, which is dependent on the chloride ion concentration (Ref 48). Furthermore, the addition of chloride ions in the solution would enhance the electrochemical activity of the steel electrode, as indicated by a negative shift of steady-state corrosion potential in Fig. 1, resulting in a high passive current density, as seen in Fig. 3. The increased electrode activity upon addition of chloride ions in the solution can also be demonstrated by the EIS measurements. In general, the one semicircle in EIS plot is attributed to the charge-transfer reaction occurring at the electrode/solution interface. The size of the semicircle is directly related to the charge-transfer resistance. It is seen from Fig. 2 that the addition of chloride ions causes a decrease of the semicircle size, and thus the charge-transfer resistance. Apparently, the activity of the electrode is enhanced.

The Mott-Schottky analysis (Fig. 6) also shows that the space-charge layer capacitance of the passive film formed in the chloride-containing solution is higher than that formed in the chloride-free solution, and simultaneously, the Mott-Schottky slope decreases. Since the donor density is inversely proportional to the slope (Ref 25-27), an addition of chloride ions in the solution results in the increase of the donor density in passive film. According to point defect model (Ref 49, 50), the oxygen vacancies may act as the primary donors in an n-type semiconductor passive film. With the increase of donor density, there are more probabilities for chloride ions to combine with oxygen vacancies to form cation vacancies, which move toward the steel/film interface, resulting in initiation of pits. Therefore, the addition of chloride ions in the solution also changes the property of the passive film, which is more prone to occurrence of pitting corrosion.

4.2 Effects of Hydrogen-Charging on Corrosion of X80 Steel in Bicarbonate-Carbonate Solution

It has been demonstrated (Ref 51) that hydrogen-charging would enhance the anodic dissolution of the steel, as shown in the present work that there is a higher passive current density (Fig. 3), a lower corrosion potential (Fig. 1) and a smaller charge-transfer resistance (Fig. 2) for the charged steel than those for a uncharged steel.

Furthermore, the present work shows that hydrogen-charging would not affect the pitting resistance, indicating that the charged hydrogen is not involved in the pitting initiation. However, the PPR tests (Fig. 5) show that hydrogen may accelerate the pit growth, as demonstrated by the increased pitting current density when the applied potential is more than E_{pit}. Even when the potential is back to the passive potential of 0.2 V (SCE), the current density continues to increase since the generated pits cannot be repassivated at this potential. The measured increment of current density upon hydrogen-charging is approximately four times of that of the uncharged steel during continuous growth of corrosion pits, as seen in Fig. 5. Moreover, previous calculations about the oxidative current density of the charged hydrogen (Ref 51, 52) has shown that the current increment due to the hydrogen oxidation is negligible, compared to the enhanced anodic dissolution current density of the steel. Therefore, it is reasonable to assume that the measured current density is primarily attributed to dissolution current density, rather than the oxidation of the charged hydrogen. When the applied potential is further back to −0.1 V (SCE), the decrease of current density is due to the partial repassivation of corrosion pits. However, the newly formed passivity on the pre-charged steel has a higher activity, as indicted by a higher passive current density, than the un-charged steel.

The involvement of hydrogen in passivity and the pit growth has been paid much attention. For example, Qin et al. (Ref 52) attributed the effect of hydrogen on the passive current density to the hydrogen-induced reduction of oxide and the decrease of the thickness of passive film. Wallinder et al. (Ref 53) proposed that the increase in the passive current density after hydrogen-charging is due to the diffusion of hydrogen atoms from the specimen surface to the film, accelerating the anodic dissolution. The present work shows that the hydrogen-charging increases the space-charge layer capacitance of the passive film and decreases the Mott-Schottky slope (Fig. 6). Therefore, the hydrogen-charging could contribute to the increase of donor density, enhancing the activity of the passive film. Once pits are initiated, i.e., the applied potential exceeds E_{pit} in this work, the charged hydrogen may accumulate at the tip of pits, enhancing

the local dissolution of steel. The pitting current density is thus increased.

Furthermore, hydrogen-charging has an apparent effect on the photo-response of the steel electrode. As seen in Fig. 7, hydrogen-charging could result in a significant increase of photo-current density compared to that of uncharged electrode. Photo illumination could enhance the activity of the steel electrode, resulting in an increase of photo-induced anodic current density. The increased photo-current density may also include the oxidative current density for the charged hydrogen atoms. When the photo illumination is turned off, the activation source disappears and the electrode recovers to its original state gradually.

5. Conclusions

A stable passivity can be established on X80 steel in carbonate-bicarbonate solution in the absence and presence of chloride ions. The hydrogen-charging does not alter the transpassive potential, but increases the passive current density. When chloride ions are contained in the solution, pitting corrosion will be initiated. The pitting potential is independent of the hydrogen-charging. The addition of chloride ions enhances the electrochemical activity of the steel electrode, as indicated by a negative shift of steady-state corrosion potential, a high passive current density, and a decrease of charge-transfer resistance. Moreover, an addition of chloride ions in the solution results in the increase of the donor density in passive film, which is more prone to occurrence of pitting corrosion.

Hydrogen-charging would enhance the anodic dissolution and electrochemical activity of the steel by increasing the donor density in the film. Hydrogen-charging does not affect the pitting potential, indicating that the charged hydrogen is not involved in the pitting initiation. However, hydrogen may accelerate the pit growth. Once pits are initiated, the charged hydrogen may accumulate at the tip of pits, enhancing the local dissolution of the steel. The pitting current density is thus increased.

Photo illumination could enhance the activity of the steel electrode, resulting in an increase of photo-induced anodic current density.

Acknowledgment

This work was supported by Canada Research Chairs Program and Natural Science and Engineering Research Council of Canada (NSERC).

References

1. M. Baker Jr., Stress Corrosion Cracking Studies, Integrity Management Program DTRS56-02-D-70036, Department of Transportation, Office of Pipeline Safety, USA, 2004
2. Canadian National Energy Board, Report of Public Inquiry Concerning Stress Corrosion Cracking on Canadian Oil and Gas Pipelines, MH-2-95, November 1996
3. R.N. Parkins, A Review of Stress Corrosion Cracking of High-Pressure Gas Pipelines, *Corrosion 2000*, NACE, Houston, 2000 (paper no. 363)
4. A.Q. Fu, X. Tang, and Y.F. Cheng, Characterization of Corrosion of X70 Pipeline Steel in Thin Electrolyte Layer Under Disbonded Coating by Scanning Kelvin Probe, *Corros. Sci.*, 2009, **51**, p 186–190
5. X. Tang and Y.F. Cheng, Localized Dissolution Electrochemistry at Surface Irregularities of Pipeline Steel, *Appl. Surf. Sci.*, 2008, **254**, p 5199–5205
6. M.C. Li and Y.F. Cheng, Corrosion of the Stressed Pipe Steel in Carbonate-Bicarbonate Solution Studied by Scanning Localized Electrochemical Impedance Spectroscopy, *Electrochim. Acta*, 2008, **53**, p 2831–2836
7. C.W. Du, X.G. Li, P. Liang, Z.Y. Liu, G.F. Jia, and Y.F. Cheng, Effects of Microstructure on Corrosion of X70 Pipe Steel in an Alkaline Soil, *J. Mater. Eng. Perform.*, 2009, **18**, p 216–220
8. F.M. Song, Predicting the Mechanisms and Crack Growth Rates of Pipelines Undergoing SCC at High pH, *Corros. Sci.*, 2009, **51**, p 2657–2674
9. R.N. Parkins, Predictive Approaches to Stress Corrosion Cracking, *Corros. Sci.*, 1980, **22**, p 147–166
10. R.N. Parkins, Realistic Stress Corrosion Crack Velocities for Life Prediction Estimates, *Life Prediction of Corrodible Structures*, Vol 1, R.N. Parkins, Ed., NACE International, Houston, TX, 1994, p 97–112
11. R.N. Parkins, Overview of Intergranular Stress Corrosion Cracking Research Activities, *Line Pipe Research Supervisory Committee of the Pipeline Research Committee of the American Gas Association*, PR-232-9401, May 1994
12. G.A. Zhang and Y.F. Cheng, Micro-Electrochemical Characterization of Corrosion of Pre-cracked X70 Pipeline Steel in a Concentrated Carbonate/Bicarbonate Solution, *Corros. Sci.*, 2010, **52**, p 960–968
13. R.N. Parkins, Conceptual Understanding and Life Prediction for SCC of Pipelines, *Proceedings of Corrosion 96, Research Topical Symposia*, P.L. Andresen and R.N. Parkins, Ed., NACE International, Houston, TX, 1996, p 1–17
14. R.N. Parkins, Prevention and Control of Stress Corrosion Cracking—An Overview, *Corrosion 1985*, NACE, Houston, 1985 (paper no. 348)
15. R.N. Parkins and R.R. Fessler, Line Pipe Stress Corrosion Cracking—Mechanisms and Remedies, *Corrosion 1986*, NACE, Houston, 1986 (paper no. 320)
16. J.A. Beavers and B.A. Harle, Mechanisms of High-pH and Near-Neutral-pH SCC of Underground Pipelines, *International Pipeline Conference*, Vol 1, ASME, 1996, p 555–568
17. D.H. Davies and G.T. Burstein, The Effects of Bicarbonate on the Corrosion and Passivation of Iron, *Corrosion*, 1980, **36**, p 416–422
18. R.N. Parkins and S. Zhou, The Stress Corrosion Cracking of C-Mn Steel in CO_2-HCO_3-CO_3^{2-} Solutions. I: Stress Corrosion Data, *Corros. Sci.*, 1997, **39**, p 159–173
19. R.N. Parkins and S. Zhou, The Stress Corrosion Cracking of C-Mn Steel in CO_2-HCO_3-CO_3^{2-} Solutions. II: Electrochemical and Other Data, *Corros. Sci.*, 1997, **39**, p 175–191
20. G. van Boven, W. Chen, and R. Rogge, The Role of Residual Stress in Neutral pH SCC of Pipeline Steels Part I: Pitting and Cracking Occurrence, *Acta Mater.*, 2007, **55**, p 29–42
21. W. Chen, F. King, and E. Vokes, Characteristics of Near Neutral pH Stress Corrosion Cracks in an X-65 Pipeline Steel, *Corrosion*, 2002, **58**, p 267–275
22. M.Z. Yang, J.L. Luo, and B.M. Patchet, Correlation of Hydrogen-Facilitated Pitting of AISI, 304 Stainless Steel to Semiconductivity of Passive Film, *Thin Solid Films*, 1999, **354**, p 142–147
23. A.A. Valeria and M.A. Christopher Brett, Characterisation of Passive Films Formed on Mild Steels in Bicarbonate Solution by EIS, *Electrochim. Acta*, 2002, **47**, p 2081–2091
24. D.G. Li, Y.R. Feng, Z.Q. Bai, J.W. Zhua, and M.S. Zheng, Influence of Temperature Chloride Ions and Chromium Element on the Electronic Property of Passive Film Formed on Carbon Steel in Bicarbonate/Carbonate Buffer Solution, *Electrochim. Acta*, 2007, **52**, p 7877–7884
25. Y.F. Cheng and J.L. Luo, Electronic Structure and Pitting Susceptibility of Passive Film on Carbon Steel, *Electrochim. Acta*, 1999, **44**, p 2947–2956
26. Y.F. Cheng and J.L. Luo, Comparison of Pitting Susceptibility and Semiconducting Properties of the Passive Films on Carbon Steel in Chromate and Bicarbonate Solutions, *Appl. Surf. Sci.*, 2000, **167**, p 113–121
27. M.D. Cunha Belo, N.E. Hakiki, and M.G.S. Ferreira, Semiconducting Properties of Passive Films Formed on Nickel-Base Alloys Type 600: Influence of the Alloying Elements, *Electrochim. Acta*, 1999, **44**, p 2473–2481

28. J.W. Schultze and M.M. Lohrengel, Stability Reactivity and Breakdown of Passive Films: Problems of Recent and Future Research, *Electrochim. Acta*, 2000, **45**, p 2499–2513
29. M.E. Armacanqui and R.A. Oriani, Effect of Hydrogen on the Pitting Resistance of Passivating Film on Nickel in Chloride-Containing, *Corrosion*, 1988, **44**, p 696–698
30. Q. Yang and J.L. Luo, Effects of Hydrogen on Disorder of Passive Films and Pitting Susceptibility of Type 310 Stainless Steel, *J. Electrochem. Soc.*, 2001, **148**, p B29–B35
31. H. Yashiro, B. Pound, N. Kumagai, and K. Tanno, The Effect of Permeated Hydrogen on the Pitting of Type 304 Stainless Steel, *Corros. Sci.*, 1998, **40**, p 781–791
32. L. Zhang, X.G. Li, C.W. Du, and Y.F. Cheng, Corrosion and Stress Corrosion Cracking Behavior of X70 Pipeline Steel in a CO_2-Containing Solution, *J. Mater. Eng. Perform.*, 2009, **18**, p 319–323
33. J.G. Yu, J.L. Luo, and P.R. Norton, Electrochemical Investigation of the Effects of Hydrogen on the Stability of the Passive Film on Iron, *Electrochim. Acta*, 2002, **47**, p 1527–1536
34. S. Ningshen, U.K. Mudali, and G. Amarend, Hydrogen Effects on the Passive Film Formation and Pitting Susceptibility of Nitrogen Containing Type 316L Stainless Steels, *Corros. Sci.*, 2006, **48**, p 1106–1121
35. G. Razzini, M. Cabrini, S. Maffi, G. Mussati, and L. Peraldo Bicelli, Photoelectrochemical Visualization in Real-Time of Hydrogen Distribution in Plastic Regions of Low-Carbon Steel, *Corros. Sci.*, 1999, **41**, p 203–209
36. G. Razzini, S. Maffi, G. Mussati, and L. Peraldo Bicelli, The Scanning Photoelectrochemical Microscopy of Diffusing Hydrogen into Metals, *Corros. Sci.*, 1995, **37**, p 1131–1141
37. G. Razzini, S. Maffi, G. Mussati, L. Peraldo Bicelli, and G. Mitsi, Photo-Electrochemical Imaging of Hydrogen-Induced Damage in Stainless Steel, *Corros. Sci.*, 1997, **39**, p 613–620
38. S. Maffi, C. Lenardi, and B. Bozzini, Photoelectrochemical Imaging of Non-Planar Surfaces: The Influence of Geometrical and Optical Factors on Image Formation, *Meas. Sci. Technol.*, 2002, **13**, p 1398–1403
39. Y.M. Zeng and J.L. Luo, Electronic Band Structure of Passive Film on X70 Pipeline Steel, *Electrochim. Acta*, 2003, **48**, p 3551–3562
40. Y.M. Zeng, J.L. Luo, and P.R. Norton, A Study of Semiconducting Properties of Hydrogen Containing Passive Films, *Thin Solid Films*, 2004, **460**, p 116–124
41. K.T. Corbett, B.R. Bowen, and C.W. Petersen, High Strength Steel Pipeline Economics, *Int. J. Offshore Polar Eng.*, 2004, **14**, p 36–38
42. G.A. Zhang and Y.F. Cheng, Micro-Electrochemical Characterization and Mott-Schottky Analysis of Corrosion of Welded X70 Pipeline Steel in Carbonate/Bicarbonate Solution, *Electrochim. Acta*, 2009, **55**, p 316–324
43. C. DeWaard and D.E. Milliams, Carbonic Acid Corrosion of Steel, *Corrosion*, 1975, **31**, p 177–181
44. J.K. Heuer and J.F. Stubbins, An XPS Characterization of $FeCO_3$ Films from CO_2 Corrosion, *Corros. Sci.*, 1999, **41**, p 1231–1243
45. J.O.M. Bockris and D. Drazic, The Electrode Kinetics of the Deposition and Dissolution of Iron, *Electrochim. Acta*, 1962, **7**, p 293–313
46. B.R. Linter and G.T. Burstein, Reaction of Pipeline Steel in Carbon Dioxide Solution, *Corros. Sci.*, 1999, **41**, p 117–139
47. P. Li, T.C. Tan, and J.Y. Lee, Impedance Spectra of the Anodic Dissolution of Mild Steel in Sulfuric Acid, *Corros. Sci.*, 1996, **38**, p 1935–1955
48. Y.F. Cheng, M. Wilmott, and J.L. Luo, The Role of Chloride Ions in Pitting of Carbon Steel Studied by Statistical Analysis of Electrochemical Noise, *Appl. Surf. Sci.*, 1999, **152**, p 161–168
49. D.D. Macdonald, Passivity—the Key to Our Metals-Based Civilization, *Pure Appl. Chem.*, 1999, **71**, p 951–986
50. D.D. Macdonald, Point Defect Model for the Passive State, *J. Electrochem. Soc.*, 1992, **139**, p 3434–3449
51. M.C. Li and Y.F. Cheng, Mechanistic Investigation of Hydrogen-Enhanced Anodic Dissolution of X-70 Pipe Steel and its Implication on Near-Neutral pH SCC of Pipelines, *Electrochim. Acta*, 2007, **52**, p 8111–8117
52. Z. Qin, P.R. Norton, and J.L. Luo, Effects of Hydrogen on Formation of Passive Films on AISI, 310 Stainless Steel, *Br. Corros. J.*, 2001, **36**, p 33–42
53. D. Wallinder, G. Hultquist, and B. Tventen, Hydrogen in Chromium: Influence on Corrosion Potential and Anodic Dissolution in Neutral NaCl Solution, *Corros. Sci.*, 2001, **43**, p 1267–1271